Neural Archetypes Learnt from Hemochromatosis Reveals Iron Dysregulation in Motor Circuits

Robert Loughnan[1,2,3,11], Jonathan Ahern[1,2], Mary Boyle[1,4], Terry L. Jernigan[1,2,5,6] , Donald J. Hagler, Jr.[3,6], John R. Iversen[2,7], Oleksandr Frei[8], Diana M. Smith[2,3], Ole Andreassen[8], Leo Sugrue[10], Wesley K. Thompson[11], Anders Dale[1,3,6,9], Andrew J. Schork[12,13,14], Chun Chieh Fan[6,11]

1. Department of Cognitive Science, University of California, San Diego, 9500 Gilman Drive, La Jolla, CA 92093, USA
2. Center for Human Development, University of California, San Diego, 9500 Gilman Drive, La Jolla, CA 92161, USA
3. Center for Multimodal Imaging and Genetics, University of California, San Diego School of Medicine, 9444 Medical Center Dr, La Jolla, CA 92037, USA
4. Johns Hopkins Bloomberg School of Public Health, 615 N. Wolfe Street, Baltimore, MD 21205, USA
5. Department of Psychiatry, University of California, San Diego School of Medicine, 9500 Gilman Drive, La Jolla, CA 92037, USA
6. Department of Radiology, University of California, San Diego School of Medicine, 9500 Gilman Drive, La Jolla, CA 92037, USA
7. Swartz Center for Computational Neuroscience, University of California, San Diego, 9500 Gilman Drive, La Jolla, CA 92161, USA
8. NORMENT Centre, Division of Mental Health and Addiction, Oslo University Hospital & Institute of Clinical Medicine, University of Oslo, Oslo, Norway
9. Department of Neuroscience, University of California, San Diego School of Medicine, 9500 Gilman Drive, La Jolla, CA 92037, USA
10. Department of Radiology and Biomedical Imaging and Department of Psychiatry, University of California, San Francisco, 505 Parnassus Avenue, San Francisco, CA 94143, USA
11. Center for Population Neuroscience and Genetics, Laureate Institute for Brain Research, Tulsa, OK 74103, USA
12. Institute of Biological Psychiatry, Mental Health Center - Sct Hans, Copenhagen University Hospital, Copenhagen, Denmark
13. Neurogenomics Division, The Translational Genomics Research Institute (TGEN), Phoenix, AZ, USA
14. Section for Geogenetics, GLOBE Institute, Faculty of Health and Medical Sciences, Copenhagen University, Copenhagen, Denmark

Abstract

Iron is a mineral crucial for cellular processes but can be neurotoxic when imbalanced. Cumulative evidence suggests motor circuitry is particularly vulnerable to neurotoxic effects of iron, as both peripheral and central iron levels have been associated with movement disorders such as Parkinson's Disease (PD)[1–7]. However, clinical trials to reduce iron levels among movement disorder patients have shown both therapeutic and pathological effects[8,9], indicating an incomplete understanding of iron dysregulation and its consequences in the human brain. In this study, we drew upon the archetypal brain pattern observed in C282Y homozygous individuals[10] who exhibit excessive absorption of dietary iron and risk of hemochromatosis[11]. The score we generated to summarize the continuum of the iron dysregulation in vulnerable brain regions from Magnetic Resonance Imaging exhibited a U-shape relationship with PD risk. Compared to individuals in the fourth quartile of scores, those in the lowest quartile of scores had an over 3-fold risk for developing PD (OR=3.19, Z=5.61, $p=2.06\times10^{-8}$), in addition to C282Y homozygotes having an over 2-fold risk for developing PD (OR=2.40, Z=3.34, $p=8.41\times10^{-4}$). Genome wide associations implicated genes involved in iron homeostasis: TF (rs6794370, $p=2.43\times10^{-81}$); HFE (rs1800562, $p=6.93\times10^{-75}$); and TMPRSS6 (rs2413450, $p=2.52\times10^{-50}$). We found these associations colocalized with gene expression of glial cells and variation in scores appeared to be driven by the peripheral iron levels. Our findings highlight the pivotal role of glial cells in balancing iron in motor circuitry, with iron depletion and overload both appearing to be related to PD risk. Disruptions in peripheral iron levels may upset the glial cells' balance, causing problems with central iron homeostasis and, in turn, motor function. We envision this is an initial step toward a more personalized approach in designing iron related therapy for movement disorders, providing iron supplement or iron chelation based on a more comprehensive understanding of brain iron dysregulation.

Introduction

Iron is an essential element required for the body to function properly, however an overload of iron can cause damage to healthy tissue[11,12]. In the central nervous system the balancing act of iron homeostasis appears to be a double-edged sword for Parkinson's Disease (PD). On the one hand: iron is a necessary cofactor required for dopamine synthesis[13] - the cardinal neurotransmitter disrupted in PD. On the other hand: high levels of iron promotes free-radical generation and can exacerbate the aggregation of Lewy body inclusions[14] - another hallmark of the disorder.

Epidemiological studies have shown a paradoxical relationship between iron levels and PD risk. Observational studies have found higher disease burden among anemic patients[1], male blood donors[2], individuals with low serum iron[3,4] and lower hemoglobin levels[5]. In contrast, high iron levels also appear to be linked with greater PD risk: with genetic mutations leading to regional brain iron accumulation and the presentation of PD or parkinsonism related conditions[6,10]. Furthermore, neuroimaging, via Magnetic Resonance Imaging (MRI), and post-mortem studies of PD brain have found higher levels of iron in motor regions (e.g., substantia nigra and red nucleus)[7].

These findings have led researchers to attempt to use iron as a therapeutic target for PD and related disorders through the use of iron chelators[15]: which are drugs that bind to and remove excess iron. Clinical trials of iron chelators have shown promise for some patients with movement disorders while exacerbating symptoms in others[8,9]. Our inability to explain this heterogeneity in treatment outcomes points to a poor understanding of iron dyshomeostasis occurring in movement disorders. An ability to identify PD subgroups related to central iron dysregulation will be necessary to illuminate the path toward innovative therapeutic avenues that are personalized, precise, and efficacious.

To investigate the role of iron in the presentation of movement disorders researchers have studied the dietary intake[16], anemic status[1] and brains of PD patients[7]. Here, we adopt an alternative approach by leveraging the regional brain iron accumulation associated with the most prevalent genetic risk factor for excessive iron absorption in the gut, known as C282Y homozygosity, to create a brain MRI endophenotype that captures a continuum of brain iron dysregulation predictive of PD risk. C282Y homozygosity, the genotype responsible for the majority of hereditary hemochromatosis cases[17], exhibits an MRI pattern showcasing substantial localized iron accumulation in the brain's motor circuits, specifically the basal ganglia and cerebellum[10]. Notably, this genotype also corresponds to a twofold increase in male-specific risk of developing movement disorders. To operationalize this MRI finding into an endophenotype, which we refer to as the "Hemochromatosis Brain", we trained a classifier to predict C282Y homozygosity status from T2-weighted brain MRI scans, a modality sensitive to iron accumulation, in a subsample of 960 individuals taken from UK Biobank (UKB). We then deploy this classifier on 35,283 independent MRI images, also from UKB, none of whom are C282Y homozygotes, to generate a PolyVoxel Score (PVS)[18] for each individual capturing the degree to which they resemble the archetypal Hemochromatosis Brain. Armed with this PVS, we aim to answer two questions. First, does a neural archetype learnt from the extreme case of iron dysregulation inform us about the genetic drivers of iron homeostasis of the human brain more generally? Second, does the degree of brain iron buildup, as encapsulated by the

Hemochromatosis Brain, predict the risk of movement disorders? This work is an important step in understanding the genetic determinants of differences in brain iron dysregulation and identifying putative iron-related subgroups of PD.

Results

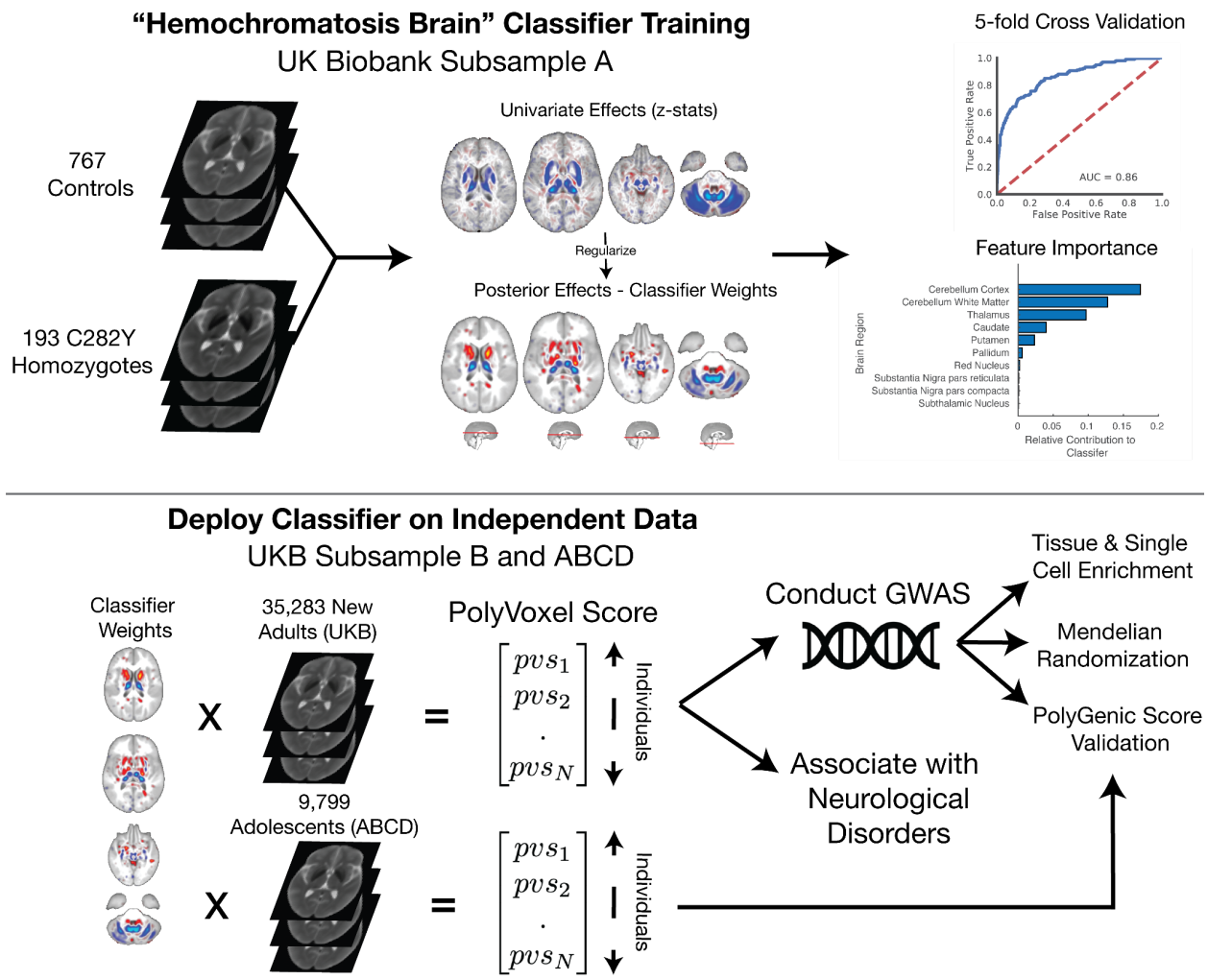

Figure 1 Overview of study design. Top panel: Hemochromatosis Brain Classifier training in Subsample A of UKB to differentiate controls from C282Y homozygotes from T2-weighted MRI scans, with univariate and regularized classifier weights, classifier performance (ROC) and feature importance by brain region. Lower panel: deploy classifier in Subsample B (UKB) and ABCD Study® to generate PolyVoxel Score (PVS) capturing Hemochromatosis Brain liability. In Subsample B we then conduct a GWAS to find variants associated with this PVS liability scale. Using these GWAS results we perform tissue and single cell enrichment analysis, mendelian randomization and polygenic score validation against the PVS generated from the ABCD Study. Finally, we test this PVS against neurological disorders within UKB.

Learning from the Hemochromatosis Brain

Figure 1 presents a graphical workflow of the analysis performed in this paper, with eTable 1 giving a demographic breakdown of each subsample. Performing 5-fold cross validation in Subsample A of UKB, consisting of 193 C282Y homozygotes and 767 covariate-matched controls, established that the Hemochromatosis Brain classifier can predict C282Y homozygosity status with high accuracy from T2-Weighted scans (attaining an AUC=0.86). eFigure 1 shows results of hyperparameter tuning. Figure 1 displays classifier weights and features importance of classifier by brain region (see also eFigure 2). As expected, univariate statistics show strong resemblance to previous work describing C282Y homozygote effect on T2-weighted signal[33]. Feature importance of posterior effects indicate that the cerebellum, thalamus, putamen and caudate have the largest contributions to the PVS.

Evaluating the Validity of the Hemochromatosis Brain with Genetic Analyses

We then sought to evaluate the validity of our scoring system by conducting a series of genetic analyses based on the Hemochromatosis Brain PVS in an independent set of individuals from UKB. First, we performed a Genome-Wide Association Study (GWAS) with the PVS in Subsample B as the phenotype of interest. For discovery we restricted this analysis to a single homogenous ancestry group, and used the remaining individuals for validation. This resulted in a discovery sample size of 30,709 European ancestry individuals and 4,608 non European ancestry individuals for replication. This analysis revealed 43 genome-wide significant loci associated with the Hemochromatosis Brain phenotype and high heritability: h^2_{ldsc} =0.381 (se=0.033) – see Figure 2A and eFigure 3. Among the top hits we found many that are known regulators of iron homeostasis: for example, rs6794370 (TF; $p=2.43\times10^{-81}$) transferrin is the principal glycoprotein responsible for mediating transport of iron through blood plasma; rs1800562 (HFE; $p=6.93\times10^{-75}$) is the same C282Y mutation on which the classifier was trained (here rediscovered with the heterozygotes); rs2413450 (TMPRSS6, $p=2.52\times10^{-50}$), TMPRSS6 is part of production signaling pathway of hepcidin, the key hormonal regulator of iron absorption in humans; rs13107325 ($p=3.66\times10^{-41}$) and rs12304921 ($p=5.05\times10^{-21}$) are linked respectively to metal transporters ZIP8 and DMT1, the latter being a gene highly expressed in the gut and previously linked with microcytic anemia with iron overload[19,20]. We found our discovered SNPs showed greatest overlap with previously studied traits relating to iron/red blood cells, brain/cognition and non iron blood markers (eFigure4), with only one SNP (rs13107325) previously linked with PD[21]. Analysis of rare genetic variants using exome burden testing revealed two genes associated with the PVS: TF ($p=5.21\text{x}10^{-8}$) and OR1J4 ($p=1.35\text{x}10^{-6}$). See extended data tables for full summary of GWAS results.

Using LDSC[22] on common variant GWAS results we found the Hemochromatosis Brain was negatively genetically correlated only with intracranial volume (r_g=-0.21, z=-5.19, $=1.7\times10^{-6}$) and no other traits tested (eFigure5). We additionally performed S-LDSC (stratified-LDSC) across 489 tissue-specific chromatin-based annotations across the body from

peaks for six epigenetic marks[23]. Results revealed the hippocampus (H3K27ac, p_{fdr}=0.014 and H3K4me1, p_{fdr}=0.025) and substantia nigra (H3k27ac, p_{fdr}=0.036) displayed a significantly enriched signal. Performing cell type enrichment using FUMA[24] of Hemochromatosis Brain GWAS using cell types defined from PsychENCODE[25] displayed an enrichment for glial cells: oligodendrocytes (p_{fdr}=6.62×10^{-5}), astrocytes (p_{fdr}=1.7×10^{-3}) and microglia (p_{fdr}=1.8×10^{-2}) and somewhat surprisingly no enrichment for neuronal cells– see Figure 2B. This pattern of enrichment exhibits a similar pattern followed by iron concentrations calculated using x-ray spectroscopy[26] – displayed in Figure 2C for comparison. Mendelian randomization[27] (MR) results between peripheral blood iron markers[28] and the PVS revealed evidence for a strong causal relationship leading from serum iron (β_{std}=0.73, p=4.91x10^{-86}) and transferrin saturation (β_{std}=0.62, p=2.97x10^{-93}) to brain iron accumulation (Figure 2D) with no evidence for the reverse relationship (eFigure 6). We additionally found significant, although weaker, MR associations of total iron binding capacity (β_{std}=-0.36, p=1.05x10^{-47}) and ferritin (β_{std}=0.342, p=1.22x10^{-16}) to brain iron accumulation as captured by the PVS, with again no evidence for the reverse direction (eFigure 6). Taken together these indicate evidence for a causal link of peripheral serum iron and transferrin saturation leading to variability in brain iron accumulation measured by the PVS. Interestingly, despite significant phenotypic associations between PVS and PD, we did not find any significant MR associations between PVS and PD, or peripheral blood iron markers and PD (Supplemental Materials, eFigure 6).

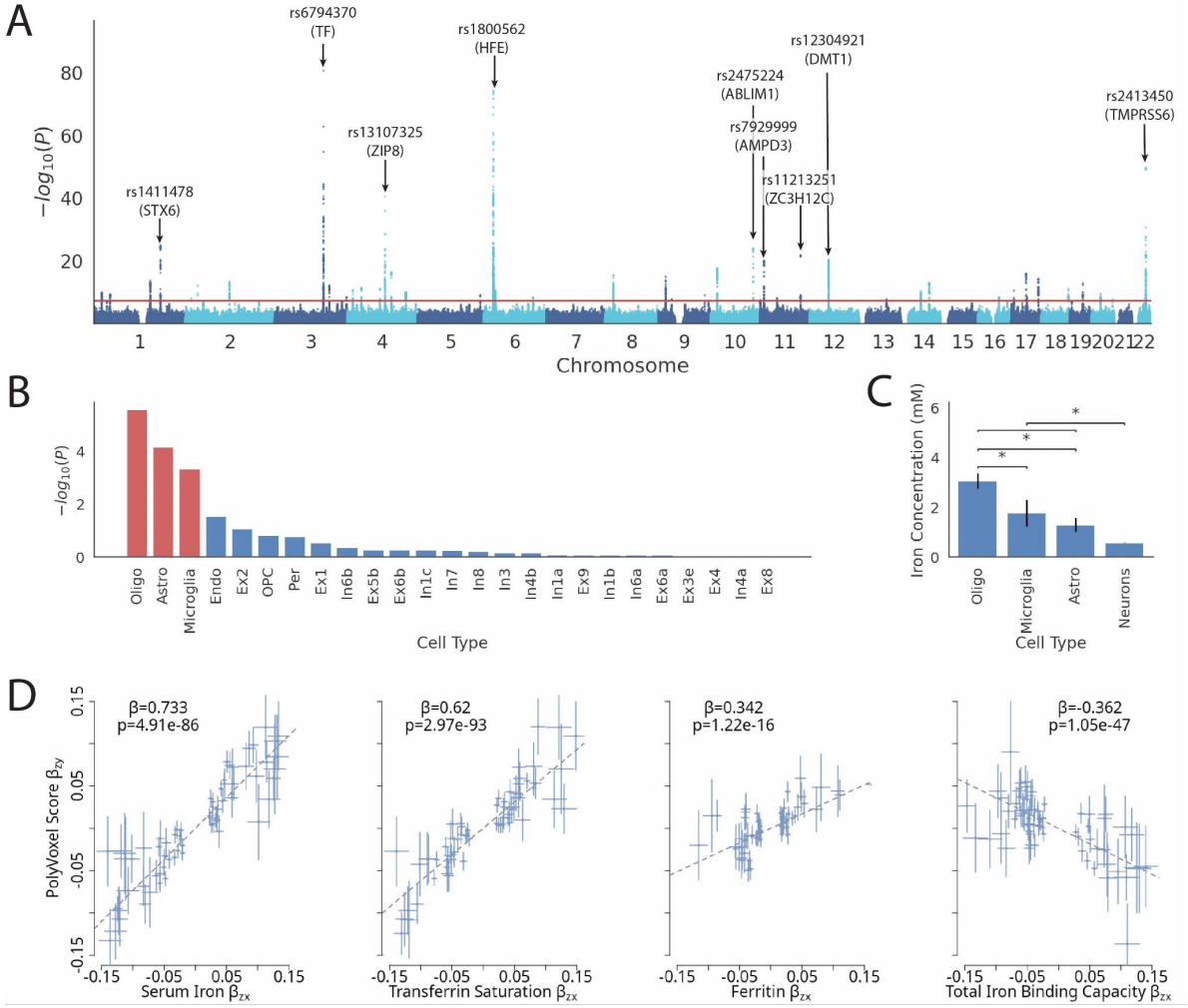

Figure 2 Results of GWAS on PVS of Hemochromatosis Brain in Subsample B. Panel A: Manhattan plot and QQ plot of GWAS result with peaks annotated – a total of 43 loci are discovered, see supplementary data tables for full list. Panel B: Brain cell type enrichment of GWAS signal using FUMA, red bars indicate FDR significantly enriched cell types. Panel C: Iron concentration (measured by using x-ray spectrometry) of cell types in rat brain with permissions from Reinert, A et. al.[26]. Panel D: Mendelian Randomization (MR) results, using GSMR, to quantify strength of causal relationship between peripheral blood iron markers and brain iron accumulation as measured by Hemochromatosis Brain PVS. Each plot shows results of conditioning on peripheral blood iron markers as exposure and PVS as outcome, reverse direction GSMR results are shown in eFigure 6.

Within our GWAS discovery we found 281 independent significant SNPs (r_{LD}<0.6). We found strong evidence of replication of these SNPs within our validation cohort of 4,608 non-European ancestry individuals from Subsample B (eTable 2) with high correlation of β estimates between these two cohorts (r=0.90, $p<1.28\times10^{-103}$) - see eFigure 7. Sign concordance between discovery and replication cohorts was high (94.6%, $p=1.0\times10^{-59}$). To test the generalization of our GWAS signal we evaluated the performance of a PolyGenic Score (PGS) to predict a PVS generated in 9,799 individuals from the ABCD Study® (aged 8-14 years old, i.e. more than 50 years younger than our training sample). Evaluating performance in separate

ancestry strata we found the PGS significantly predicted the PVS (EUR: r^2=0.018, z=12.67, p=8.01x10^{-37}; AFR: r^2=0.0086, z=2.73, p=6.33x10^{-3}, MIX: r^2=0.0069, z=5.47, p=4.41x10^{-8}). To further understand PVS changes across the lifespan, within ABCD (full sample) and UKB (subsample B), we visualize the effect of age and sex - shown in eFigure 8. Despite the much smaller age range of ABCD vs UKB, we find a notably larger age effect in ABCD (z=53.2, r^2=0.16, p<10^{-100}) than in UKB (z=-4.00, r^2=4.46x10^{-4}, p=7.29x10^{-5}) with females appearing to be phase advanced in the adolescent age range (z=27.0, r^2=0.048, p<10^{-100}). In sum, these results demonstrate that the genetics underlying the Hemochromatosis Brain PVS are detectable across the lifespan (8-80 years old) and that there are notable age-related changes in early adolescence.

Iron Homeostasis in Human Brain and Neurological Disorders

After establishing the genetic determinants of the Hemochromatosis Brain, we next examined if this novel measure was associated with any neurological disorders, in particular Parkinson Disorder (PD). We found the PVS in Subample B (containing no C282Y homozygotes) significantly and specifically predicted reduced risk for PD in this sample (OR=0.73, Z=-2.62, p=0.0089) and showed trending associations for Abnormalities of Gait and Mobility (OR=0.88, Z=-1.85, p=0.064) – see Figure 3A and eTable 4. The associations were specific to movement disorders, as we did not find evidence of a PVS association with diagnoses of any other neurological disorders tested. Performing quantile weighted regression to predict PD status in Subsample C (Figure 3B and eTable 5) we see higher risk at the two ends of the estimated brain iron concentration spectrum: with the 1st PVS quantile (OR=3.19, Z=5.61, p=2.06x10^{-8}) and C282Y homozygotes (OR=2.40, Z=3.34, p=8.41x10^{-4}). For Figure 3B mean iron concentrations for brain areas used to calculate PVS were estimated from T2* imaging for each PVS quantile and C282Y homozygotes separately to plot values on the x axis. In contrast to C282Y homozygotes, who exhibited excessive iron accumulation and twofold increased risk for PD, the PVS exhibited an inverse relationship between brain iron concentration and PD risk, indicating the critical role of iron homeostasis in maintaining the function of motor circuits. Note for Figure 3B, although there appears to be a U-shape relationship, a far greater proportion of individuals are present in the iron deplete range than in the iron overload range; each blue point represents a quantile (~25% of the cohort) while the orange point represents ~0.6% of the cohort.

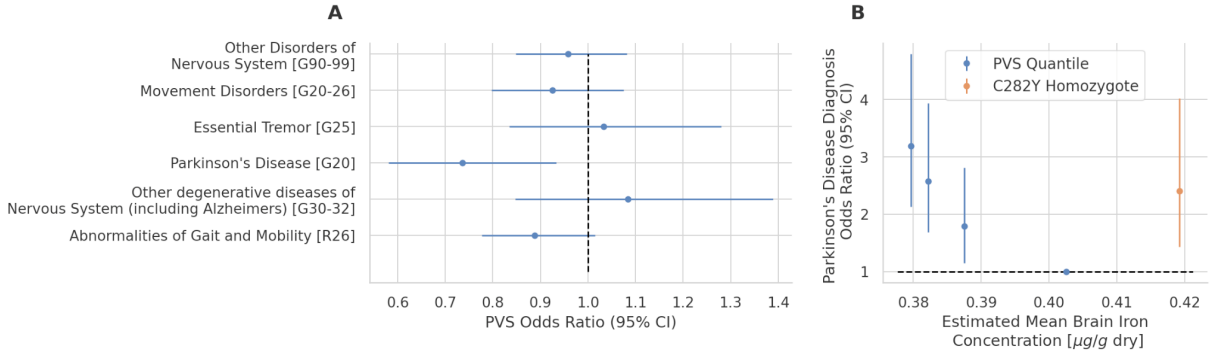

Figure 3 Association of PolyVoxel Score (PVS) with neurological diagnoses in Subsample B. Panel A: PVS odds ratio predicting each neurological disorder. Panel B: PVS quantile weighted regression in Subsample C, each point represents a categorical factor indicating one of four PVS quantile (blue) or C282Y homozygosity (orange). C282Y homozygote group represents individuals across the whole UKB sample (193 with imaging and 2,695 without imaging). Weighted regression was performed to account for 3.88 fold depletion of PD cases in imaging sample (blue) vs full sample (orange) - see methods. Regression (y-axis) was performed using PVS from T2-W, x-axis is an estimate of mean brain iron concentration using T2 imaging for each group.*

Discussion

Here, we have presented a continuum of iron homeostasis localized to motor circuits of the brain which is predictive of risk for PD. We have shown that this dysregulation spectrum is strongly associated with genetic variation (h^2_{snp}=0.381), with variants in genes known to be key regulators of iron homeostasis. Furthermore, the signal was enriched in gene expression patterns of glial cells – a cell group known to have highest concentrations of iron in the brain[26]. Additionally, MR analysis showed that iron markers in peripheral blood have a strong influence on brain iron accumulation differences. Yet the PD risk profile exhibited a U shape, indicating iron homeostasis is more relevant than absolute iron concentration. These results outline the genetic drivers, mediated through glial cells, influencing iron regulation in the brain and the putative consequences of disrupting this system. Taken together, these results indicate subgroups of PD that relate to the hormetic nature of iron in the brain, in which both depleted and excess levels can impart toxic effects, likely via different mechanisms[13,14,29].

The results from this analysis validate an established relationship between iron and movement disorders, while providing a novel biomarker for PD risk. Previous *post mortem* and *in vivo* imaging studies have found higher iron deposition in substantia nigra, putamen and red nucleus[7]; these regions have small but non-zero weights contributing to the Hemochromatosis Brain classifier (eFigure 2). Of note, there is a paucity of *in vivo* imaging results of PD results reporting on the cerebellum[7] - a region which displays the largest contribution to the PVS and which has been shown to have lower iron levels in post mortem PD brain samples[7], consistent with our findings. Additionally, deficits in iron have also been associated with movement disorders, with anemic patients and male blood donors being more likely to suffer from PD[1,2]. Furthermore, a class of rare genetic mutations result in a disease called Neurodegeneration with Brain Iron Accumulation (NBIA) which presents with a stereotyped pattern of iron accumulation in the basal ganglia similar to the univariate pattern observed in the Hemochromatosis Brain. The clinical presentation of this disorder is of dystonia and other Parkinsonism symptoms. Moreover, in the context of the MTMP model, which is the most extensively researched animal model of Parkinson's disease (PD), it seems that ferroptosis, a form of cell death that relies on iron, has emerged as a key mechanism responsible for causing the motor symptoms associated with movement disorders[29]. The work presented in the manuscript once again underscores the link between iron dysregulation in the brain and the risk of developing a movement disorder.

Although epidemiological, imaging and postmortem studies suggest a link between PD and iron, GWAS of the disorder have not uncovered a major contribution from iron[30]. Indeed, in our study we only find one independent significant SNP (rs13107325, $p=3.66\times10^{-41}$)

overlapping with variants previously associated with PD. We also find that the Hemochromatosis Brain does not display any genetic correlation with the largest previous GWAS of PD (eFigure 5). Our interpretation of this result is that iron dysregulation may represent one potential contributor to PD risk and without this subtype being identified in current PD GWAS these unmodelled heterogeneous genetic effects lead to null findings for iron related variants. This idea of genetic heterogeneity is thought to explain the modest GWAS results of Major Depression[31], and we aim to investigate this possibility in future work. Much of the current PD results highlight lysosomal dysfunction as a principal mechanism underlying disease pathopysiology[32]. The contribution of iron dysregulation to PD risk may still converge on lysosomal dysfunction. For example, iron depletion or overload leading to oxidative stress and cell death resulting ultimately in disease presentation; this process could be exacerbated in patients with pre-existing lysosomal dysfunction.

Iron chelators (drugs that facilitate the removal of iron from the body) have recently been used as a potential therapeutic target for movement disorders with mixed outcomes. In the treatment of NBIA, iron chelation with deferiprone has shown promise in improving symptom progression[8]. Conversely, a phase 2 randomized control trial of deferiprone in 372 PD patients was stopped early due to worsening symptom progression from treatment[9]. These results may be consistent with our findings if NBIA and PD represent two ends of the iron dysregulation spectrum. With this view the more rare cases of NBIA result from iron overload thereby benefiting from iron chelation. This is in contrast to PD in the general population which may lie in the more iron-deplete range thereby being exacerbated by chelation therapy. In this interpretation NBIA would align with the risk profile of C282Y homozygotes and PD patients with the lower PVS quantiles in Figure 3B. In support of this view we see the bulk of the UKB imaging sample lies in the iron-deplete range of PD risk with each of the four blue points of Figure 3B representing ~25% of the sample and C282Y homozygotes representing 0.06%. This indicates that future iron based interventions may benefit from MRI based patient stratification, such as through the use of the Hemochromatosis Brain PVS, enabling targeted treatment.

Single cell enrichment analysis implicated glial, and not neuronal, cells as the principal cell class associated with our Hemochromatosis Brain GWAS results. This is consistent with findings that glial cells, particularly oligodendrocytes, show larger concentrations of iron than neuronal cell types[26,33] and is also consistent with the role of glial cells' in maintaining brain homeostasis[34]. Although our results indicate glial cells appear to mediate the central disruption of iron homeostasis, the consequences of this disruption may be borne by other cell classes. Indeed dopamine neurons, with a strong dependency on iron for dopamine synthesis[13] and mitochondrial function[35], may represent a cell class particularly sensitive to this disruption. Further, despite glial cells being widespread across the brain, our analysis of tissue enrichment across the human body found our GWAS signal to be localized only to the substantia nigra and hippocampus. The former being rich in dopaminergic neurons and the primary site of PD pathology[35], and the latter known to show accelerated atrophy in PD[36]. These provide further support the view that the Hemochromatosis Brain represents an iron specific endophenotype of relevance to PD.

Analysis revealed a genetic signature of the Hemochromatosis Brain appears to be generalizable across a 50 year age span from adolescence (ABCD) to late adulthood (UK Biobank) . Within ABCD we also observed a larger change in PVS scores as a function of age than for UK Biobank (eFigure 8) - this recapitulates previous findings of brain iron accumulation exhibiting an early exponential pattern with the largest increases observed in the first two decades of life[37]. As others have suggested[38] this may be indicative of the development of the dopaminergic system, which relies heavily on iron. In addition, along this developmental trajectory we find evidence that females appear to phase advanced when

compared to males - a pattern which is observed for other markers during adolescence[39,40]. It is possible that early life differences in regional brain iron that we detect predisposes individuals to different neurological risk profiles later in life.

An important limitation of the current study is its observational nature. Although, T2-weighted MRI signal is known to be related to iron concentrations[41], and the GWAS signal we detect appears to implicate iron related genes with encouragingly strong MR results, we cannot conclude that iron specifically is imparting a causal impact on disease risk for PD. It is possible that iron may be serving as a marker for another biological process that is responsible for generating the differential risk for PD. In addition, T2-weighted signal is not solely reduced by higher iron concentrations; processes of edema and gliosis also impact T2-weighted intensity[42]. Moreover, manganese similarly shortens T2-weighted signal and is known to accumulate in the basal ganglia as a result of liver cirrhosis which is common with peripheral iron overload[43]. It is possible that some of the effects captured by the PVS are in fact related to these non-iron processes. Finally, due to correlations between brain regions and the regularization process during training of our PVS some brain regions flip signs (compare univariate statics and posterior weights in Figure 1 and eFigure 2). The PVS approach's strength and weakness lie in its ability to condense a complex signal into one instrumental variable, indicative of a continuum of brain iron dysregulation. Although, in general, higher PVS values indicate more iron accumulation in net, this doesn't ensure that iron levels in each individual brain region align with this direction.

Here we have showcased a continuum of neural iron dysregulation related to PD risk and which underscores the hormetic nature of this vital element. We have demonstrated that this continuum is strongly influenced by both genetic drivers and peripheral markers of iron. We hope that this dysregulation spectrum may be useful in patient stratification and in understanding heterogeneity in treatment outcomes. To this end we provide weights and code to easily calculate PVS for suitable MRI scans within new datasets - see methods. Our novel approach could be applied more broadly to other archetype learning scenarios, providing a framework for greater biological interpretation of multivariate measures.

1. Savica, R. *et al.* Anemia or low hemoglobin levels preceding Parkinson disease. *Neurology* **73**, 1381 LP – 1387 (2009).
2. Logroscino, G., Chen, H., Wing, A. & Ascherio, A. Blood donations, iron stores, and risk of Parkinson's disease. *Mov. Disord.* **21**, 835–838 (2006).
3. Pichler, I. *et al.* Serum Iron Levels and the Risk of Parkinson Disease: A Mendelian Randomization Study. *PLOS Med.* **10**, e1001462 (2013).
4. Medeiros, M. S. *et al.* Iron and Oxidative Stress in Parkinson's Disease: An Observational Study of Injury Biomarkers. *PLOS ONE* **11**, e0146129 (2016).
5. Deng, Q. *et al.* Lower hemoglobin levels in patients with parkinson's disease are associated with disease severity and iron metabolism. *Brain Res.* **1655**, 145–151 (2017).

6. Hayflick, S. J., Kurian, M. A. & Hogarth, P. Chapter 19 - Neurodegeneration with brain iron accumulation. in *Neurogenetics, Part I* (eds. Geschwind, D. H., Paulson, H. L. & Klein, C. B. T.-H. of C. N.) vol. 147 293–305 (Elsevier, 2018).
7. Wang, J. Y. *et al.* Meta-analysis of brain iron levels of Parkinson's disease patients determined by postmortem and MRI measurements. *Sci. Rep.* **6**, 1–13 (2016).
8. Klopstock, T. *et al.* Safety and efficacy of deferiprone for pantothenate kinase-associated neurodegeneration: a randomised, double-blind, controlled trial and an open-label extension study. *Lancet Neurol.* **18**, 631–642 (2019).
9. Devos, D. *et al.* Trial of Deferiprone in Parkinson's Disease. *N. Engl. J. Med.* **387**, 2045–2055 (2022).
10. Loughnan, R. *et al.* Association of Genetic Variant Linked to Hemochromatosis with Brain Magnetic Resonance Imaging Measures of Iron and Movement Disorders. *JAMA Neurol.* **79**, 919–928 (2022).
11. Powell, L. W., Seckington, R. C. & Deugnier, Y. Haemochromatosis. *The Lancet* **388**, 706–716 (2016).
12. Pasricha, S.-R., Tye-Din, J., Muckenthaler, M. U. & Swinkels, D. W. Iron deficiency. *The Lancet* **397**, 233–248 (2021).
13. Ramsey, A. J., Hillas, P. J. & Fitzpatrick, P. F. Characterization of the Active Site Iron in Tyrosine Hydroxylase: REDOX STATES OF THE IRON*. *J. Biol. Chem.* **271**, 24395–24400 (1996).
14. Angelova, P. R. *et al.* Alpha synuclein aggregation drives ferroptosis: an interplay of iron, calcium and lipid peroxidation. *Cell Death Differ.* **27**, 2781–2796 (2020).
15. Kulshreshtha, D., Ganguly, J. & Jog, M. Iron Chelation in Movement Disorders: Logical or Ironical. *Can. J. Neurol. Sci.* **48**, 752–759 (2021).
16. Logroscino, G., Gao, X., Chen, H., Wing, A. & Ascherio, A. Dietary Iron Intake and

Risk of Parkinson's Disease. *Am. J. Epidemiol.* **168**, 1381–1388 (2008).

17. Bomford, A. Genetics of haemochromatosis. *Lancet* **360**, 1673–1681 (2002).

18. Loughnan, R. J. *et al.* Generalization of cortical MOSTest genome-wide associations within and across samples. *NeuroImage* **263**, 119632 (2022).

19. Beaumont, C. *et al.* Two new human DMT1 gene mutations in a patient with microcytic anemia, low ferritinemia, and liver iron overload. *Blood* **107**, 4168–4170 (2006).

20. Bardou-Jacquet, E. *et al.* A novel N491S mutation in the human SLC11A2 gene impairs protein trafficking and in association with the G212V mutation leads to microcytic anemia and liver iron overload. *Blood Cells. Mol. Dis.* **47**, 243–248 (2011).

21. Smeland, O. B. *et al.* Genome-wide Association Analysis of Parkinson's Disease and Schizophrenia Reveals Shared Genetic Architecture and Identifies Novel Risk Loci. *Biol. Psychiatry* **89**, 227–235 (2021).

22. Bulik-Sullivan, B. *et al.* LD score regression distinguishes confounding from polygenicity in genome-wide association studies. *Nat. Genet.* **47**, 291–295 (2015).

23. Finucane, H. K. *et al.* Heritability enrichment of specifically expressed genes identifies disease-relevant tissues and cell types. *Nat. Genet.* **50**, 621–629 (2018).

24. Watanabe, K., Taskesen, E., van Bochoven, A. & Posthuma, D. Functional mapping and annotation of genetic associations with FUMA. *Nat. Commun.* **8**, 1826 (2017).

25. Wang, D. *et al.* Comprehensive functional genomic resource and integrative model for the human brain. *Science* **8464**, (2018).

26. Reinert, A., Morawski, M., Seeger, J., Arendt, T. & Reinert, T. Iron concentrations in neurons and glial cells with estimates on ferritin concentrations. *BMC Neurosci.* **20**, 1–14 (2019).

27. Zhu, Z. *et al.* Causal associations between risk factors and common diseases inferred from GWAS summary data. *Nat. Commun.* **9**, 224 (2018).

28. Bell, S. *et al.* A genome-wide meta-analysis yields 46 new loci associating with biomarkers of iron homeostasis. *Commun. Biol.* **4**, (2021).

29. Do Van, B. *et al.* Ferroptosis, a newly characterized form of cell death in Parkinson's disease that is regulated by PKC. *Neurobiol. Dis.* **94**, 169–178 (2016).

30. Nalls, M. A. *et al.* Identification of novel risk loci, causal insights, and heritable risk for Parkinson's disease: a meta-analysis of genome-wide association studies. *Lancet Neurol.* **18**, 1091–1102 (2019).

31. Flint, J. & Kendler, K. S. The Genetics of Major Depression. *Neuron* **81**, 484–503 (2014).

32. Navarro-Romero, A., Montpeyó, M. & Martinez-Vicente, M. The Emerging Role of the Lysosome in Parkinson's Disease. *Cells* **9**, 1–25 (2020).

33. Connor, J. R. & Menzies, S. L. Relationship of iron to oligodendrocytes and myelination. *Glia* **17**, 83–93 (1996).

34. Jäkel, S. & Dimou, L. Glial cells and their function in the adult brain: A journey through the history of their ablation. *Front. Cell. Neurosci.* **11**, 1–17 (2017).

35. Muñoz, Y., Carrasco, C. M., Campos, J. D., Aguirre, P. & Núñez, M. T. Parkinson's Disease: The Mitochondria-Iron Link. *Park. Dis.* **2016**, 7049108 (2016).

36. Poewe, W. *et al.* Parkinson disease. *Nat. Rev. Dis. Primer* **3**, 1–21 (2017).

37. Camicioli, R. *et al.* Parkinson's disease is associated with hippocampal atrophy. *Mov. Disord. Off. J. Mov. Disord. Soc.* **18**, 784–790 (2003).

38. Aquino, D. *et al.* Age-related Iron Deposition in the Basal Ganglia: Quantitative Analysis in Healthy Subjects. *Radiology* **252**, 165–172 (2009).

39. Larsen, B. *et al.* Maturation of the human striatal dopamine system revealed by PET and quantitative MRI. *Nat. Commun.* **11**, 846 (2020).

40. Lim, S., Han, C. E., Uhlhaas, P. J. & Kaiser, M. Preferential Detachment During

Human Brain Development: Age- and Sex-Specific Structural Connectivity in Diffusion Tensor Imaging (DTI) Data. *Cereb. Cortex* **25**, 1477–1489 (2015).

41. Wolf, R. M. & Long, D. Pubertal development. *Pediatr. Rev.* **37**, 292–300 (2016).

42. Ordidge, R. J., Gorell, J. M., Deniau, J. C., Knight, R. A. & Helpern, J. A. Assessment of relative brain iron concentrations using T2-weighted and T2*-weighted MRI at 3 Tesla. *Magn. Reson. Med.* **32**, 335–341 (1994).

43. Prayson, R. *Neuropathology*. (2011).

44. Grochowski, C. *et al.* Serum iron, Magnesium, Copper, and Manganese Levels in Alcoholism: A Systematic Review. *Mol. Basel Switz.* **24**, 1361 (2019).

45. Von Elm, E. *et al.* The Strengthening the Reporting of Observational Studies in Epidemiology (STROBE) statement: Guidelines for reporting observational studies. *Epidemiology* **18**, 800–804 (2007).

46. Alfaro-Almagro, F. *et al.* Image processing and Quality Control for the first 10,000 brain imaging datasets from UK Biobank. *NeuroImage* **166**, 400–424 (2018).

47. Das, S. *et al.* Next-generation genotype imputation service and methods. *Nat. Genet.* **48**, 1284 (2016).

48. Taliun, D. *et al.* Sequencing of 53,831 diverse genomes from the NHLBI TOPMed Program. *Nature* **590**, 290–299 (2021).

49. Fuchsberger, C., Abecasis, G. R. & Hinds, D. A. minimac2: faster genotype imputation. *Bioinformatics* **31**, 782–784 (2015).

50. Conomos, M. P., Miller, M. B. & Thornton, T. A. Robust inference of population structure for ancestry prediction and correction of stratification in the presence of relatedness. *Genet. Epidemiol.* **39**, 276–293 (2015).

51. Fan, C. C. *et al.* Genotype Data and Derived Genetic Instruments of Adolescent Brain Cognitive Development Study® for Better Understanding of Human Brain Development.

Behav. Genet. **53**, 159–168 (2023).

52. Chen, C.-Y. *et al.* Improved ancestry inference using weights from external reference panels. *Bioinformatics* **29**, 1399–1406 (2013).

53. Auton, A. *et al.* A global reference for human genetic variation. *Nature* **526**, 68–74 (2015).

54. Reich, D. *et al.* Reconstructing Native American Population History. *Nature* **488**, 370–374 (2012).

55. Watts, R. *et al.* The Adolescent Brain Cognitive Development (ABCD) study: Imaging acquisition across 21 sites. *Dev. Cogn. Neurosci.* **32**, 43–54 (2018).

56. Hagler, D. J. *et al.* Image processing and analysis methods for the Adolescent Brain Cognitive Development Study. *NeuroImage* **202**, (2019).

57. Jovicich, J. *et al.* Reliability in multi-site structural MRI studies: Effects of gradient non-linearity correction on phantom and human data. *NeuroImage* **30**, 436–443 (2006).

58. Wald, L., Schmitt, F. & Dale, A. Systematic spatial distortion in MRI due to gradient non-linearities. *NeuroImage* **13**, 50 (2001).

59. Wells, W. Multi-modal volume registration by maximization of mutual information. *Med. Image Anal.* **1**, 35–51 (1996).

60. Henninger, B., Alustiza, J., Garbowski, M. & Gandon, Y. Practical guide to quantification of hepatic iron with MRI. *Eur. Radiol.* **30**, 383–393 (2020).

61. Chang, C. C. *et al.* Second-generation PLINK: rising to the challenge of larger and richer datasets. *GigaScience* **4**, (2015).

62. Mbatchou, J. *et al.* Computationally efficient whole-genome regression for quantitative and binary traits. *Nat. Genet.* **53**, 1097–1103 (2021).

63. Cingolani, P. *et al.* A program for annotating and predicting the effects of single nucleotide polymorphisms, SnpEff. *Fly (Austin)* **6**, 80–92 (2012).

64. de Leeuw, C. A., Mooij, J. M., Heskes, T. & Posthuma, D. MAGMA: Generalized Gene-Set Analysis of GWAS Data. *PLoS Comput. Biol.* **11**, 1–19 (2015).

65. Watanabe, K., Umićević Mirkov, M., de Leeuw, C. A., van den Heuvel, M. P. & Posthuma, D. Genetic mapping of cell type specificity for complex traits. *Nat. Commun.* **10**, (2019).

66. Finucane, H. K. *et al.* Partitioning heritability by functional annotation using genome-wide association summary statistics. *Nat. Genet.* **47**, 1228–1235 (2015).

67. Roadmap Epigenomics Consortium *et al.* Integrative analysis of 111 reference human epigenomes. *Nature* **518**, 317–329 (2015).

68. Dunham, I. *et al.* An integrated encyclopedia of DNA elements in the human genome. *Nature* **489**, 57–74 (2012).

69. Ge, T., Chen, C. Y., Ni, Y., Feng, Y. C. A. & Smoller, J. W. Polygenic prediction via Bayesian regression and continuous shrinkage priors. *Nat. Commun.* **10**, 1–10 (2019).

Methods

UK Biobank Sample

Genotypes, MRI scans, demographic and clinical data were obtained from the UK Biobank under accession number 27412, excluding 206 participants who withdrew their consent. All participants provided electronic signed informed consent and the study was approved by the UK Biobank Ethics and Governance Council. The recruitment period for participants was from 2006 to 2010, and participants had to be 40-69 years old during this period to be included in the sample. For the current study we analyzed data from a total sample of 38,937 individuals (20,435 females) with a mean age of 64.3 years (standard deviation 7.6 years) for analysis. This sample was made up of individuals who had qualified imaging (36,243 individuals) and/or who were C282Y homozygotes (2,888 individuals). We split the sample of individuals with qualified imaging into two non-overlapping groups: Subsample A for C282Y homozygote classifier training and Subsample B for deploying this classifier. A final group, subsample C, was used for weighted quantile regression (see below) which was Subsample B

with the addition of all 2,888 C282Y homozygotes from the whole UKB sample. eTable 1 summarizes demographics of these three subsamples. Genotype, health record and neuroimaging data was collected from January 2006 to May 2021. Data analysis was conducted from January 2022 to October 2022. This study follows the Strengthening the Reporting of Observational Studies in Epidemiology (STROBE) reporting guideline for cross-sectional studies[45].

UK Biobank Image acquisition

T1 weighted and diffusion weighted scans were collected from three scanning sites throughout the United Kingdom, all on identically configured Siemens Skyra 3T scanners, with 32-channel receiver head coils. For diffusion scans, multiple scans with no diffusion gradient were collected (b=0 s/mm^2) to fit diffusion models. The average of these b=0s/mm^2 scans was used as voxel-wise measures of T2-weighted intensities. Diffusion-weighted scans were collected using a SE-EPI sequence at 2mm isotropic resolution. T1-weighted scans were collected using a 3D MPRAGE sequence at 1mm isotropic resolution. Voxelwise T2* values were estimated as part of the susceptibility-weighted imaging protocol at a voxel resolution of 0.8 × 0.8 × 3 mm and with 2 echoes (echo times, 9.42 and 20 milliseconds). To reduce noise, T2* images were spatially filtered (3 × 3 × 1 median filtering followed by limited dilation to fill missing data holes). If a person had multiple (longitudinal) scans we used the first scan. Further details of image acquisition can be found here[46].

ABCD Sample®

The ABCD study is a longitudinal study across 21 data acquisition sites following 11,878 children starting at 9 and 10 years old. This paper analyzed the baseline and year 2 follow up sample from data release 4.0 (NDA DOI:10.15154/1523041). The ABCD study used school-based recruitment strategies to create a population-based, demographically diverse sample with heterogeneous ancestry. Genotype data was imputed using the TOPMED imputation server[47–49] and genetic principal components were estimated using PC-AIR[50] as described elsewhere[51]. We selected individuals who had passed neuroimaging and genetic quality control checks. We calculated participants' continental genetic ancestry as calculated using SNPweights[52] and aligning with 1k Genomes Project[53], and indigenous reference panels[54]. Each individual was assigned an ancestry proportion to 4 continental groups: European (EUR), African (AFR), Native American (AMR), South Asian (SAS) or East Asian (EAS). From this participants were categorized into one of the three largest ancestry groups of European (EUR), African (AFR) and admixed (MIX). Individuals were categorized as EUR or AFR if they exceeded 80% ancestry within one of these continental ancestry groups and MIX if they were less than 80% ancestry across all groups. This resulted in 5,977 EUR, 687 AFR, and 3,135 MIX individuals for performing ancestry stratified analysis - see eTable 2 for demographic details.

ABCD Image acquisition

T1-weighted (T1w) and diffusion-weighted MRI (dMRI) scans were collected using Siemens Prisma and Prisma Fit, GE Discovery 750 and Phillips Achieva and Ingenia 3T scanners. Scanning protocols were harmonized across 21 acquisition sites. Full details of harmonization routines have been described elsewhere[55,56]. T1w images were acquired using a 3D MPRAGE scan at 1mm isotropic resolution. dMRI scans were acquired in the axial plane at 1.7mm isotropic resolution, with seven b=0s/mm^2 frames. The average of b=0s/mm^2 scans was taken as voxel-wise measures of T2-weighted intensities.

Image Preprocessing

Scans were corrected for nonlinear transformations provided by MRI scanner manufacturers[57,58]. T2-weighted and T2* scans (for UKB) were registered to T1-weighted images using mutual information[59]. Intensity inhomogeneity correction was performed by applying smoothly varying, estimated B1-bias fields[56]. Images were rigidly registered and resampled into alignment with a pre-existing, in-house, averaged, reference brain with 1.0 mm isotropic resolution[56]. Atlases used to define regions of interest for classifier feature importance analysis are shown in eTable 3.

C282Y Homozygote Classifier and PolyVoxel Score Generation

We aimed to train a classifier to predict C282Y homozygosity status from MRI scans. For training we generated a sample derived from the 193 C282Y homozygotes with qualified imaging and found covariate matched controls at a ratio of 4:1 (cases to controls). Controls were matched for sex, age, scanner and top ten principal components of genetic ancestry. This was performed as described elsewhere with the exception that controls were selected as those with no C282Y mutations (i.e. C282Y heterozygotes were excluded from being cases or controls). This resulted in a subsample of 193 C282Y “cases” (112 female) and 767 “controls” (463 female), i.e. no C282Y mutations, for training the classifier – we refer to this sample as Subsample A - see eTable 2 for description. For fitting, hyperparameter tuning and evaluating the classifier we employed a 5 fold cross-validation scheme in Subsample A.

The C282Y homozygote classifier was fitted using a PolyVoxel Score (PVS) framework[18] as follows. Let $\boldsymbol{X}^{train}$ represent the pre-residualized imaging matrix with *N* rows of individuals and *M* columns of voxels in the training sample. Each element of this matrix, $x_{i,j}^{train}$ represents the voxel intensity for the i-th individual at the j-th voxel for a T2-weighted scan. Here each column in $\boldsymbol{X}^{train}$ was quantile transformed to a normal distribution and pre-residualized for

covariates of age, sex, MRI scanner and top 10 principal components of genetics. Let $\boldsymbol{y}^{train}$ represent the 1-dimensional vector such that:

$$y^{train} = \begin{cases} 1, & \text{if C282Y homozygote} \\ 0, & \text{otherwise} \end{cases}$$

We then regress each column of $\boldsymbol{X}^{train}$ with $\boldsymbol{y}^{train}$ to generate a vector of univariate z-statistics, $\boldsymbol{z}$, of dimension *M* – where each element describes the univariate association of that voxel with C282Y homozygosity status. We then threshold this $\boldsymbol{z}$ to restrict to nominally significant voxels in which p<0.01. Next, we could use the vector to generate out of sample PVS's from a test sample's imaging data, to estimate liability of individuals along the Hemochromatosis Brain liability scale as follows: $\hat{\boldsymbol{y}}^{test} = \boldsymbol{z}\boldsymbol{X}^{test}$ (these univariate statistics are displayed in Figure 1). However, due to the correlation structure across voxels this gives suboptimal out of sample prediction. As such we use the correlation matrix of $\boldsymbol{X}^{train}$, $\boldsymbol{R}$, to re-weight $\boldsymbol{z}$ to obtain posterior effect sizes. $\boldsymbol{R}$ can be decomposed using singular value decomposition $\boldsymbol{R} = \boldsymbol{U}\boldsymbol{S}\boldsymbol{U}^T$ ($\boldsymbol{U}$ – unitary matrix, $\boldsymbol{S}$ – diagonal matrix with singular values on its diagonal). We consider the regularized form of $\boldsymbol{R}$ as: $\boldsymbol{R}_r = \boldsymbol{U}\boldsymbol{S}_r\boldsymbol{U}^T$, where $\boldsymbol{S}_r$ is obtained from $\boldsymbol{S}$ by keeping r largest singular values and replacing the remaining with r^{th} largest. We then decorrelate association statistics to generate PVS classifier weights (posterior effects in Figure 1) as $\boldsymbol{w}_r = \boldsymbol{R}_r^{-1}\boldsymbol{z}$ which were in turn are used to generate PVS scores for each individual as: $\hat{\boldsymbol{y}}_r^{test} = \boldsymbol{w}_r\boldsymbol{X}^{test}$. During cross-validation in Subsample A, nine $\hat{\boldsymbol{y}}_r^{test}$ were generated with different values of (1, 5, 10, 20, 50, 100, 200, 500, 1000 and M (i.e. no regularization)). The r value that maximized the association between and $r = 13$ was selected for displaying the receiver operator characteristic (ROC) curve in Figure 1. For downstream analysis in subsample B we used the mean optimal value, $r = 13$, to fit posterior weights across the whole of subsample A.

To capture feature importance of the classifier and univariate weights for different brain regions (Figure 1 and eFigure 2), we normalized $\boldsymbol{z}$ and $\boldsymbol{w}_r$ to be of unit length as $\tilde{\boldsymbol{z}}$ and $\tilde{\boldsymbol{w}}_r$. We then calculated the sum of squares of $\tilde{\boldsymbol{z}}$ and $\tilde{\boldsymbol{w}}_r$ for each voxel that fell within a given brain region (see eTable 3 for atlases used to define brain regions). For plotting results of weighted quantile regression (Figure 3B) we estimated mean iron concentration was calculated for each individual by taking the mean across p<0.01 voxels from T2* imaging[60]. We then used previously published estimates linking R2* (1/T2*) values to iron concentration as [μg/g dry] = C × R2*[Hz] / 3.2, where C = 2000 / 36.

Genome Wide Association of Hemochromatosis Brain

In Subsample B we then performed a GWAS with the Hemochromatosis Brain PVS as the phenotype of interest, covarying for age, sex and top ten components of genetic ancestry. We restricted this analysis to individuals declared as self-identified "White British" and similar genetic ancestry (using Data Field: 22006), this resulted in 30,709 individuals. 4,608 remaining

individuals from Subsample B were used for replication of GWAS discoveries. Additionally, to enable the calculation of genetic correlations of related traits in UK Biobank, we performed GWAS for intracranial volume, as a measure of brain size, and 4 red blood cell traits: mean corpuscular volume, mean corpuscular hemoglobin, mean sphere cell volume and hemoglobin concentration. If there were multiple instances of a variable we took their mean value for each subject. For these measures, as well as the PVS, we quantile transformed them to a normal distribution to enforce normality and reduce leverage of outliers. We used sample and variant QC's of: --geno 0.05, --hwe 1e-12, --maf 0.005 and --mind 0.1 using PLINK (v2.00a3.6LM)[61]. This resulted in 7,131,446 remaining variants and no individuals removed. PLINK was used for performing GWAS across these 6 traits (using –glm). For discovered variants we performed validation in 4,608 individuals who self-identified in any other category as "White British" by performing the same process for GWAS discovery. Using independent significant SNPs (see locus definition below) from the discovery set we evaluated replication in two ways: 1) compared/correlated coefficients and 2) evaluated sign concordance of coefficients between discovery and replication cohorts. For 2) we used a binomial test to assess the significance of in proportion of sign concordant SNPs.

Gene Burden Analysis Using Whole Exome Data

To test if rare genetic variants were associated with variability in brain iron levels captured by the Hemochromatosis Brain PVS we performed gene burden analysis using Reginie (v3.1.1)[62]. For this analysis we had 19,498 individuals from Subsample B with available genetic data. Using annotations from SnpEff[63] (v5.0) of each observed mutation we applied a mask of mutations labeled as high or moderate consequence. Using parameters of --aaf-bins 0.1,0.05,0.01 and --bsize 200, and the same covariates described above we associated each binary gene burden score with variability in PVS. Across 18,860 genes tested we defined discoveries as those whose p-value exceeded Bonferroni significance of 0.05/18,860.

GWAS Locus Definition and Discovery Overlap GWAS Catalog

Summary statistics were uploaded to FUMA (FUMA: v1.4.1, MAMGA v1.08)[24] for locus definition and gene mapping. "Independent significant SNPs" represent genome-wide significant SNPs that are in moderate to low LD with one another (r_{LD}<0.6). "Genome-wide loci" represent regions in which independent significant SNPs are merged if they are: a) in moderate LD with one another (r_{LD}>0.1) or b) are physically close to one another (<250kb). FUMA provides an output of independent significant SNPs and reports which of these overlap with previous studies reported in GWAS catalog (e104_r2021-09-15). We use this to define broad categories of studies that overlapped with our discoveries, see eTable 4 for search terms used to define categories. We allowed each significant SNP to be counted for multiple categories if it appeared in different studies across categories. However, we ensured that it was not counted more than once within a specific category, even if it appeared in multiple studies within that category. The results of this analysis are shown in eFigure 4 and extended data tables.

Mendelian Randomization

To assess the causal strength of association between peripheral blood markers, PD and brain iron dysregulation as measured by the Hemochromatosis Brain we conducted mendelian randomization using GSMR[27]. In order to conduct these analyses we used previous GWAS summary statistics of serum iron, transferrin saturation, total iron binding capacity, ferritin[28], and parkinson's disease[30]. Linkage disequilibrium (LD) was estimated from the 30,709 UK Biobank individuals used for the PVS GWAS; this LD was then used to find independent significant SNPs to use as instruments for GSMR. The following parameters were used: gwas_thresh=$5x10^{-8}$, single_snp_hedi_thresh=0.01, multi_snps_hedi_thresh=0.01, heidi_outlier_flag=T, ld_r2_thresh=0.05, ld_fdr_thresh=0.05. Bivariate GSMR was run (in both directions) to confirm the directionality of causation.

Single Cell Enrichment

We performed cell type enrichment using the FUMA platform[24]. Association statistics at the gene level were calculated using MAGMA (v1.08)[64]. This gene-based distribution was then associated with expression patterns of 25 cell types from PsychENCODE single-cell RNA-seq data collected from the adult brain[25] by performing a gene-property analysis[65].

Tissue-Specific Enrichment

We used stratified LDSC (S-LDSC)[66] to examine tissue-type specific enrichment of the Hemochromatosis Brain GWAS results. We analyzed annotations derived from 489 tissue-specific chromatin assays of bulk tissue from peaks for six epigenetic marks. These data were collected as part of the Roadmap Epigenomics and ENCODE projects[67,68], annotations were downloaded from previous analysis[23] (see URLs). We controlled for baseline annotations as recommended by S-LDSC[66]. We reported the signed enrichment Z statistics, as well as the corresponding FDR corrected multiple comparisons adjusted p-values.

Polygenic/PolyVoxel Score Validation

We tested the generalization of both our genetic and neuroimaging findings of the Hemochromatosis Brain to individuals from the ABCD cohort: a cohort on average more than 50 years younger than the UKB cohort from which these findings were discovered. Within the ABCD sample we generate a PVS score for each individual at each available time point. This included 9,799 individuals at baseline (age 8.9-11.1 years) and 4,615 at 2 year follow up (age 10.58-13.67years). To generate polygenic scores we calculated posterior effect sizes using PRScs[69] using the LD estimated from the 1k Genome European ancestry reference panel (N=503). Polygenic scores were then calculated by applying these posterior effect sizes using ‘plink –score’ (v2.00) to ABCD genetic data. Performing ancestry stratified analysis (within the groups described above) we fitted linear mixed effect models to predict the PVS of each individual with fixed effects of sex, age, top 10 PCs of genetic ancestry, and a categorical variable indicating the mri software and serial number. We included random intercepts for

subject id (to account for longitudinal measures) nested with family id membership. Variance explained was computed as $r^2 = \frac{t^2}{t^2 + DF}$, where DF is the degrees of freedom.

Disease Enrichment of Hemochromatosis Brain

We wanted to test the utility and specificity of the Hemochromatosis Brain PVS in distinguishing cases and controls of PD and other disorders of the brain. To do this we defined Subsample B in UK Biobank who were the remainder of individuals with neuroimaging that were not in Subsample A. This resulted in 35,283 individuals (18,278 females, 0 C282Y homozygotes). For this sample we generated a PVS for each individual from their imaging data using the C282Y homozygote classifier, as described above, trained in the full Subsample A (regularization parameter set to r=13 as the mean optimal value across cross-validation). This PVS is a single score per individual that in essence quantifies the degree of iron dysregulation in motor circuits observed in C282Y homozygotes. We then associated this Hemochromatosis Brain PVS with 6 disorders/classes of disorders of the brain using logistic models with covariates of age, sex, scanning site and top ten components of genetic ancestry. These 6 different disorders/categories were: Other disorders of the Nervous System (ICD10: G90-99), Movement Disorders (ICD10: G20-G26), Parkinson's Disease (ICD10: G20), Essential Tremor (ICD10:G25), Other degenerative diseases of the Nervous System (including Alzheimer's) (ICD10: G30-32) and Abnormalities of Gait and Mobility (ICD10: R26). These diagnoses were extracted from UK Biobank field 41270.

Quantile Weighted Regression

Individuals were assigned to one of 4 quantiles 1-4 according to their PVS with 1st being the lowest 25% of PVS, 2nd being scores between 25th and 50th percentile and so on. We aimed to quantify the PD risk of each of these quantiles with reference to C282Y homozygotes taken from the whole UKB sample, including those that did not have neuroimaging (2,888 homozygotes taken from 488,288 individuals). In order to accomplish this we needed to account for the observed 3.88 fold depletion of PD cases in the neuroimaging cohort vs the whole UKB sample (compare columns A + B with full sample of eTable 1). We achieved this by performing weighted regression assigning a weight of 3.88 to PD cases in the neuroimaging cohort and 1 to all other individuals. A model was then (within sample C of eTable 1) fit to predict PD from these quantiles and C282Y homozygote status as categorical variables covarying for the same covariates described above. We then used estimated mean iron concentrations for PVS brain regions, as described above, to display the mean of this value for each group as shown on the x axis of Figure 3B.

Data Availability: UK Biobank data was accessed under accession number 27412. Summary statistics from GWAS of Hemochromatosis Brain PVS are available for download. Researchers can apply for access to UK Biobank data at

https://www.ukbiobank.ac.uk/enable-your-research/apply-for-access. The ABCD data used in this came from [NIMH Data Archive Digital Object Identifier (10.15154/1523041)]. This data is available to approved researchers, find more information at https://abcdstudy.org.

Code Availability: We have created a python command line program to generate PVS's for T2-Weighted images registered in Montreal Neurological Institute space using classification weights presented in this analysis - https://github.com/robloughnan/pvs.

UK Biobank Acknowledgment: UK Biobank's research resource is a major contributor in the advancement of modern medicine and treatment, enabling better understanding of the prevention, diagnosis and treatment of a wide range of serious and life-threatening illnesses – including cancer, heart diseases and stroke. UK Biobank is generously supported by its founding funders the Wellcome Trust and UK Medical Research Council, as well as the Department of Health, Scottish Government, the Northwest Regional Development Agency, British Heart Foundation and Cancer Research UK. The organization has over 150 dedicated members of staff, based in multiple locations across the UK.

ABCD Acknowledgment:

Data used in the preparation of this article were obtained from the Adolescent Brain Cognitive Development℠ Study (ABCD Study®) (https://abcdstudy.org), held in the NIMH Data Archive (NDA). This is a multisite, longitudinal study designed to recruit more than 10,000 children age 9–10 and follow them over 10 years into early adulthood. The ABCD Study is supported by the National Institutes of Health and additional federal partners under award numbers:

U01DA041022, U01DA041028, U01DA041048, U01DA041089, U01DA041106, U01DA041117, U01DA041120, U01DA041134, U01DA041148, U01DA041156, U01DA041174, U24DA041123, and U24DA041147

A full list of supporters is available at https://abcdstudy.org/federal-partners/. A listing of participating sites and a complete listing of the study investigators can be found at https://abcdstudy.org/principal-investigators.html. ABCD Study consortium investigators designed and implemented the study and/or provided data but did not necessarily participate in analysis or writing of this report. This manuscript reflects the views of the authors and may not reflect the opinions or views of the NIH or ABCD Study consortium investigators.

The ABCD data repository grows and changes over time. The ABCD data used in this came from [NIMH Data Archive Digital Object Identifier (10.15154/1523041)].

URLS

PLINK (https://www.cog-genomics.org/plink/2.0/)
FUMA (https://fuma.ctglab.nl)
LDSC and sLDSC (https://github.com/bulik/ldsc)

Annotations for sLDSC tissue-specific analysis
(https://alkesgroup.broadinstitute.org/LDSCORE/)

Funding: This work was supported by grants R01MH122688 and RF1MH120025 funded by the National Institute for Mental Health (NIMH) in addition to Lundbeck Foundation fellowship (R335-2019-2318).

Conflict of Interest Statement: Dr. Andreassen has received speaker's honorarium from Lundbeck, and is a consultant to HealthLytix. Dr. Dale is a Founder of and holds equity in CorTechs Labs, Inc, and serves on its Scientific Advisory Board. He is a member of the Scientific Advisory Board of Human Longevity, Inc. and receives funding through research agreements with General Electric Healthcare and Medtronic, Inc. The terms of these arrangements have been reviewed and approved by UCSD in accordance with its conflict of interest policies. The other authors declare no competing interests.